Precision Electroweak Tests at LEP

E. Falk
Lund University, Box 118, S-221 00 Lund
Sweden

Abstract

A presentation is given of a selection of the electroweak precision tests that have been carried out at LEP. Measurements of the Z^0 lineshape and asymmetries from the LEP1 era as well as measurements of the W mass from LEP2 are described, and up-to-date results presented. A brief overview is given of some experimental aspects that are crucial to the precision tests. Radiative corrections and some of the constraints that they impose on the Standard Model are discussed.

OPEN-98-024
15/12/98

1 Introduction

LEP has operated successfully since 1989, with steady improvements in its performance and increased integrated luminosity for each year. When the data taking at and in the vicinity of the Z^0 pole, $\sqrt{s} = 91$ GeV, finished in 1995, each of the four LEP experiments had collected an integrated luminosity of about 160 pb^{-1}, and together they had recorded approximately 20 million Z^0 bosons. This wealth of statistics has allowed unprecedented testing of the electroweak theory of the Standard Model, and the results obtained have been in excellent agreement with the model, leaving only small openings for any new physics beyond the Standard Model.

The LEP2 era started in the summer of 1996 with collisions at the threshold for W^+W^- production, $\sqrt{s} = 161$ GeV. The experiments each recorded about 10 pb^{-1} during this period. Later in the year, the energy was increased to $\sqrt{s} = 172$ GeV, and another 10 pb^{-1} were recorded by each experiment. In 1997 the energy was increased further to $\sqrt{s} = 183$ GeV, and the integrated luminosity at this energy reached about 55 pb^{-1} per experiment. The higher energies of LEP2 allow a range of precision tests of the Standard Model with W pairs, including a good determination of the mass of the W boson.

Section 2 presents a selection of the tests of the electroweak theory carried out at the Z^0 pole. A summary of the measurements of beam energy and luminosity, crucial to the precision of the electroweak tests, is given in Section 3. Section 4 contains a short introduction to the measurements of the W mass. Section 5 briefly discusses radiative corrections and presents some examples of how they are used to put constraints on the Standard Model.

2 Z^0 Lineshape Measurements and Asymmetries

2.1 Z^0 Lineshape

The Z^0 lineshape measurements consist of a series of measurements of cross sections of the production of different fermions at different energy points around the Z^0 resonance. The parameters that one has chosen to extract from these measurements are the mass of the Z^0 boson, m_Z, the total width, Γ_Z, the peak hadronic cross section, σ_h^0 and the ratios of partial widths for leptons, R_e, R_μ and R_τ, defined as $R_e \equiv \Gamma_h/\Gamma_{ee}$, where Γ_h is the partial width for decay into hadrons and Γ_{ee} the partial width for decay into an electron-positron pair, and analogously for the μ and τ leptons. When lepton universality is assumed, one quotes instead $R_l \equiv \Gamma_h/\Gamma_{ll}$, where l denotes charged leptons. This particular parameter choice has the advantages that the parameters are nearly statistically independent; they are easily related to basic electroweak parameters, such as coupling strengths; and they are also easily related to specific experimental errors. m_Z, Γ_Z and σ_h^0 also have a close correspondence to the position, the width and the height of the Z^0 resonance curve as a function of energy.

The parameters are extracted through a fit to a function describing the total cross section for decay into a pair of fermions, $e^+e^- \to f\bar{f}$, as a function of s, the square of the centre-of-mass energy:

$$\sigma_f(s) = \sigma_f^0 \frac{s\Gamma_Z^2}{(s-m_Z^2) + \frac{s^2\Gamma_Z^2}{m_Z^2}} + \gamma + \gamma Z^0, \tag{1}$$

where σ_f^0 is the peak cross section for decay into a fermion pair. The terms γ and γZ^0 represent contributions from photon exchange and $\gamma - Z^0$ interference. These contributions are small relative to that of Z^0 exchange at the Z^0 pole, $\mathcal{O}(1\%)$ [1], and are fixed to their Standard-Model values in the fit. Before the function is compared with the experimental results, it is convoluted with a function describing QED corrections (mainly initial-state radiation). The peak cross section for decay into fermions is defined as

$$\sigma_f^0 \equiv \frac{12\pi\Gamma_e\Gamma_f}{m_Z^2\Gamma_Z^2}. \tag{2}$$

Using this and

$$\Gamma_Z = \sum \Gamma_f,$$

one can extract the partial widths Γ and the ratios R from the fitted parameters. The current values of the lineshape parameters, where the results of the four LEP experiments have been averaged, are presented in Table 1.

Parameter	Average Value
m_Z (GeV)	91.1867 ± 0.0020
Γ_Z (GeV)	2.4948 ± 0.0025
σ_h^0 (nb)	41.486 ± 0.053
R_e	20.757 ± 0.056
R_μ	20.783 ± 0.037
R_τ	20.823 ± 0.050
R_l	20.775 ± 0.027

Table 1: Average lineshape parameters from the preliminary results of the four LEP experiments [2], [3], [4].

An important aspect of the Standard Model that is tested in the lineshape measurements is that of lepton universality. The partial widths Γ_l are proportional to the vector and axial-vector couplings g_{Vf} and g_{Af} of the Z^0 to fermions according to

$$\Gamma_f = \frac{G_F m_Z^3}{6\pi\sqrt{2}} \left(g_{Vf}^2 + g_{Af}^2\right), \tag{3}$$

where G_F is the Fermi constant. As a consequence thereof, the ratios R_e, R_μ and R_τ should be the same if the couplings to the different lepton flavours are the same. Lepton universality is excellently confirmed by the LEP experiments, with good agreement between the different ratios R, as shown in Table 1.

Another test of the Standard Model is to count the number of light neutrino species. This is done at LEP by measuring the invisible decay width $\Gamma_{inv} = N_\nu\Gamma_\nu$, where N_ν is the number of neutrino species and Γ_ν the partial width for decay into a neutrino-antineutrino pair. N_ν is determined from

$$N_\nu = \frac{\Gamma_l}{\Gamma_\nu}\frac{\Gamma_{inv}}{\Gamma_l} = \frac{\Gamma_l}{\Gamma_\nu}\left(\sqrt{\frac{12\pi R_l}{m_Z^2\sigma_h^0}} - R_l - 3\right), \tag{4}$$

where one uses the fact that

$$\Gamma_Z = \sum \Gamma_f = \Gamma_h + 3\Gamma_l + \Gamma_{inv} \tag{5}$$

and the definition of the peak cross section (eq. 2). The ratio Γ_{inv}/Γ_l is the measured quantity, and Γ_l/Γ_ν is taken from the Standard Model. The number of neutrinos measured in this way is

$$\boxed{N_\nu = 2.993 \pm 0.011.}$$

A different approach to this measurement is instead to assume that the number of neutrinos is 3 and extract an upper limit for additional invisible decays of the Z^0 by adding a term $\Delta\Gamma_{inv}$ to the fit. Limiting the result to include only positive values of $\Delta\Gamma_{inv}$ yields the upper limit

$$\boxed{\Delta\Gamma_{inv} < 2.8 \text{ MeV at } 95\% \text{ C.L.}}$$

2.2 Asymmetries

The asymmetries that are measured at LEP have their origin in the fact that neutral-current couplings are different for left-handed and for right-handed fermions:

$$\begin{aligned} g_{Lf} &= I^3_{Lf} - Q_f \sin^2\theta_W \\ g_{Rf} &= -Q_f \sin^2\theta_W, \end{aligned} \tag{6}$$

where g_{Lf} and g_{Rf} are the couplings to left-handed and right-handed fermions respectively, I^3_{Lf} and Q_f the weak isospin and the charge of the fermion and θ_W the electroweak mixing angle. This difference leads to polarisation effects and to forward-backward asymmetries that can be measured at LEP.

Using the relations

$$\begin{aligned} g_{Vf} &= g_{Lf} + g_{Rf} \\ g_{Af} &= g_{Lf} - g_{Rf}, \end{aligned} \tag{7}$$

one can express the difference in the neutral-current coupling in terms of the chiral-coupling asymmetry $\mathcal{A}_f$ defined as

$$\mathcal{A}_f \equiv \frac{g^2_{Lf} - g^2_{Rf}}{g^2_{Lf} + g^2_{Rf}} = \frac{2 g_{Vf} g_{Af}}{g^2_{Vf} + g^2_{Af}}. \tag{8}$$

The chiral-coupling asymmetry manifests itself in different ways that can be measured experimentally: There are the so-called left-right asymmetries, which require longitudinally polarised e^+e^- beams and which are measured at SLD; there are the forward-backward asymmetries, which are measured at LEP for the three lepton flavours and for b and c quarks; there are the polarisation asymmetries, which the LEP experiments measure for the τ lepton; and there are hadronic jet charge asymmetries. The charge asymmetries and the forward-backward asymmetries for quarks will not be discussed further here.

2.3 Forward-Backward Asymmetries

The forward-backward asymmetry A_{FB} for the process $e^+e^- \to Z^0 \to f\bar{f}$ is defined as

$$A_{FB}(s) = \frac{\sigma_F(s) - \sigma_B(s)}{\sigma_F(s) + \sigma_B(s)}, \tag{9}$$

where $\sigma_{F(B)}$ denotes the cross section for the antifermion emerging in the forward (backward) direction from the interaction point, the forward direction being that of the incoming positron (see Figure 1). The forward-backward asymmetry enters the polar-angular dependence of the cross section:

$$\frac{d\sigma}{d(\cos\theta)} = 1 + \cos^2\theta + \frac{8}{3} A_{FB} \cos\theta. \tag{10}$$

At LEP, where the beams are longitudinally unpolarised, one measures the forward-backward asymmetry at the Z^0 pole:

$$A_{FB}(s = m_Z^2) \simeq A^{0,f}_{FB} \equiv \frac{3}{4} \mathcal{A}_e \mathcal{A}_f, \tag{11}$$

where $A_{FB}^{0,f}$ is called the pole asymmetry. With polarised beams one can measure the left-right asymmetry A_{LR}, which is defined as

$$A_{LR} \equiv \frac{\sigma_L - \sigma_R}{\sigma_L + \sigma_R} \simeq \mathcal{A}_e, \tag{12}$$

where σ_L and σ_R refer to the cross sections for Z^0 decays for left- and right-polarised beams respectively. As mentioned previously, this measurement is carried out at SLD.

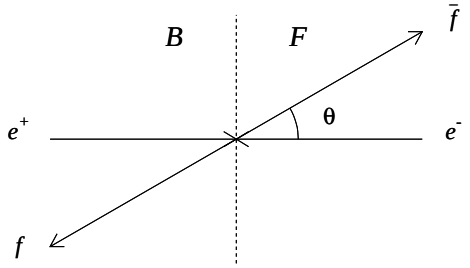

Figure 1: Definition of polar angle in e^+e^- collisions.

The forward-backward asymmetries are extracted from fits to the angular distribution of events at each energy point. The e^+e^- final state receives a significant contribution from t-channel e^+e^- (Bhabha) scattering and must be corrected for this.

The asymmetry measurements provide another important test to lepton universality; the pole asymmetries for the different lepton flavours must be the same if their gauge couplings are the same:

$$A_{FB}^{0,e} = A_{FB}^{0,\mu} = A_{FB}^{0,\tau}. \tag{13}$$

Also in this respect LEP data show strong evidence for lepton universality (see Table 2).

Parameter	Average Value
$A_{FB}^{0,e}$	0.0160 ± 0.0024
$A_{FB}^{0,\mu}$	0.0163 ± 0.0014
$A_{FB}^{0,\tau}$	0.0192 ± 0.0018
$A_{FB}^{0,l}$	0.0171 ± 0.0010

Table 2: Forward-backward asymmetries without and with lepton universality; average results from the four LEP experiments.

2.4 τ Polarisation

The τ polarisation $\mathcal{P}_\tau$ is defined as

$$\mathcal{P}_\tau \equiv \frac{\sigma_R - \sigma_L}{\sigma_R + \sigma_L}, \tag{14}$$

where $\sigma_{R(L)}$ is the cross section for a τ pair with the τ^- being right-(left-)handed. The chiral-coupling asymmetries $\mathcal{A}_e$ and $\mathcal{A}_\tau$ are extracted from the polar-angular dependence of the polarisation:

$$\mathcal{P}_\tau\,(\cos\theta) \simeq -\frac{\mathcal{A}_\tau + \frac{2\cos\theta}{1+\cos^2\theta}\mathcal{A}_e}{1 + \frac{2\cos\theta}{1+\cos^2\theta}\mathcal{A}_e\mathcal{A}_\tau}. \tag{15}$$

The polarisation of the τ lepton is measured through reconstruction of the kinematic parameters of its decay products. Five different decay modes are used: $\tau \to e\nu\bar{\nu}$; $\tau \to \mu\nu\bar{\nu}$; $\tau \to \pi\nu$; $\tau \to \rho\nu$; and $\tau \to a_1\nu$. The decay channels involving a π or a ρ yield the best sensitivity; the channel involving an a_1 has a relatively small branching fraction, and the purely leptonic channels have their polarisation signal diluted due to the fact that the two neutrinos involved in the decay prevent reconstruction of the decay angles. The experimental challenge lies in distinguishing between the different decay modes; the decay products of the τ are very well collimated due to the high momentum of the τ. The coupling asymmetries extracted from the τ polarisation measurements at LEP also show strong support for lepton universality (see Table 3).

Parameter	Average Value
$\mathcal{A}_e$	0.1399 ± 0.0073
$\mathcal{A}_\tau$	0.1411 ± 0.0064

Table 3: Chiral-coupling asymmetries from τ polarisation measurements; average results from the four LEP experiments.

2.5 Effective Couplings of the Z^0 Boson to Leptons

The data from the partial widths, the lepton forward-backward asymmetries and the τ polarisation can be combined to determine the effective couplings g_{Vl} and g_{Al} of the Z^0 to charged leptons. The couplings to the neutrinos can be measured from the invisible width of the Z^0, Γ_{inv}, under the assumptions that there are three identical neutrino generations ($\Gamma_{inv} = 3\Gamma_\nu$) and $g_{V\nu} \equiv g_{A\nu} \equiv g_\nu$. The averaged results, assuming lepton universality, for the effective couplings are given in Table 4. Figure 2 shows the 68% probability contours in the $g_{Al} - g_{Vl}$ plane.

Parameter	Average Value
g_{Vl}	-0.03681 ± 0.00085
g_{Al}	-0.50112 ± 0.00032
g_ν	$+0.50125 \pm 0.00092$

Table 4: Effective couplings of the Z^0 boson to leptons from LEP measurements of partial widths, lepton forward-backward asymmetries and τ polarisation. Lepton universality is assumed.

The asymmetry measurements determine the ratio g_{Vl}/g_{Al}, and the results are often expressed in terms of the effective electroweak mixing angle $\sin^2\theta_W^{eff}$ defined as

$$\sin^2\theta_W^{eff} \equiv \frac{1}{4}\left(1 - \frac{g_{Vl}}{g_{Al}}\right). \tag{16}$$

This definition of the electroweak mixing angle is convenient because it absorbs vertex corrections for leptons. The results of these determinations are shown in Table 5.

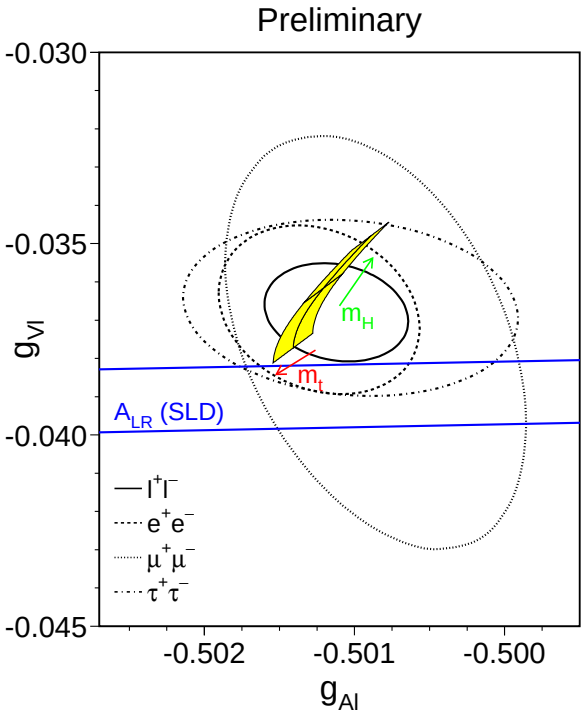

Figure 2: Contours of 68% probability in the $g_V - g_A$ plane from measurements of asymmetries and partial widths at LEP. The solid contour shows the result from a fit assuming lepton universality. Also included is the one-standard-deviation band from left-right asymmetry measurements at SLD. The shaded region shows the Standard-Model prediction for a top mass of $m_t = 175.6 \pm 5.5$ GeV and a Higgs mass of $m_H = 300^{+700}_{-240}$ GeV. The arrows point in the direction of increasing values of m_t and m_H.

3 Experimental Aspects

The high precision of the LEP experiments require very accurate measurements of the beam energy and of the luminosity. The main contribution to the error on the Z^0 mass comes from the uncertainty of the absolute beam energy, while the error on the Z^0 width is related to the uncertainty of the difference in centre-of-mass energies around the Z^0 pole. Accurate knowledge of the luminosity is crucial to the precision of the cross-section measurements.

3.1 Measurements of Beam Energy

Beam energy is measured at LEP through a method called resonant depolarisation [5], [7], which is the cornerstone in the determination of the beam energy. However, several corrections to the value measured by resonant depolarisation must be made before a final value of the energy is obtained. Resonant depolarisation makes use of the fact that transverse spin polarisation builds up naturally in e^+e^- storage rings through interaction of the electrons or positrons with the magnetic guide field, the so-called Sokolov-Ternov effect. The beam is depolarised by an applied oscillating magnetic field, which is made to resonate with the spin precession of the polarised beam electrons. The number of spin precessions per turn is proportional to the average beam energy. Such calibrations are typically performed at the end of physics fills, although they were less frequent in the early days of LEP. The intrinsic accuracy of the method is of the order of 200 keV [8].

	$\sin^2\theta_W^{eff}$
$A_{FB}^{0,l}$	0.23102 ± 0.00056
$\mathcal{A}_\tau$	0.23228 ± 0.00081
$\mathcal{A}_e$	0.23243 ± 0.00093
$A_{FB}^{0,b}$	0.23237 ± 0.00043
$A_{FB}^{0,c}$	0.2315 ± 0.0011
$< Q_{fb} >$	0.2322 ± 0.0010
Average(LEP)	0.23199 ± 0.00028
A_{LR} (SLD)	0.23055 ± 0.000412
Average(LEP+SLD)	0.23152 ± 0.00023

Table 5: Effective electroweak mixing angle determined from different asymmentry measurements. For comparison, values obtained from forward-backward asymmetries with b and c quarks and from charge asymmetries are also included, as well as the result from left-right asymmetry measurements at SLD.

Ground motion, due to terrestrial tides, heavy rainfalls, etc., causes the energy of LEP to vary with time, because the circumference is altered so that the ideal orbit no longer passes through the centre of the quadrupoles. The variation of the energy due to ground motion is about 10 MeV [9]. Therefore, the beam orbit is continually monitored during the physics periods.

The beam energy is extracted from a model that is based on the resonant-depolarisation measurement and which takes into account the beam-orbit measurements as well as other terms correcting for variations in, for example, RF cavity voltages, magnetic dipole fields and temperatures. The determination of the beam energy at LEP1 according to this method results in an uncertainty of 1.5 MeV in the Z^0 mass; the uncertainty in the Z^0 width is also 1.5 MeV [3].

The method of resonant depolarisation is not directly applicable at LEP2 energies; it becomes very difficult to achieve sufficient polarisation at beam energies above 45 GeV. Energy calibrations based on resonant polarisation are performed at lower energies, and the results are extrapolated to LEP2 energies. The extrapolation is based on magnetic-field measurements. The resulting uncertainty of the LEP energy is 30 MeV; however, the knowledge of the beam energy is less crucial at LEP2 than at LEP1 [4], [10].

3.2 Luminosity

The determination of luminosity at LEP is based on counting Bhabha events at low angles. Bhabha scattering is t-channel e^+e^- scattering, a well-known QED process with a large event rate and little dependence on the parameters to be measured in the precision tests. The differential cross section of the process has a steep angular dependence, $1/\theta^3$, which places high requirements on the electromagnetic calorimeters that are used as luminosity monitors. They must have good energy resolution; their geometrical acceptance must be known very precisely; and they must be very accurately positioned around the beam pipe on either side of the experiments. The inner edge of the monitors must be known with a precision better than 100 μm in order to match the statistical accuracy. Shifts in the location of the interaction point and in the beam alignment must also be carefully followed. The experimental uncertainty is now below 0.1% [9], which is smaller than the theoretical uncertainty of about 0.11% [3] in the calculation of the Bhabha cross section. The precision of the Bhabha cross section is currently limited by the lack of calculations of higher-order corrections.

4 Measurements of W Mass

The measurements of the W mass are treated elsewhere in these proceedings; therefore, only a brief indication of the principles and the results is given here.

Three channels are involved in the production of W pairs through $e^+e^- \to W^+W^-$ at LEP: s-channel exchange of a photon or a Z^0 and t-channel exchange of a neutrino ν_e. The decay modes are $W^+W^- \to q\bar{q}q\bar{q}$ with a branching ratio of 45.6%; $W^+W^- \to q\bar{q}l\nu$ with a branching ratio of 43.8% and $W^+W^- \to l\nu l\nu$ with a branching ratio of 10.6% [1].

At energies just above the threshold for W-pair production, the W mass is measured through the cross section for W production, which has its maximum sensitivity to the W mass in this region. The measured cross section is compared with the predicted cross section as a function of the W mass. Consequently, this method was used for the data collected at $\sqrt{s} = 161$ GeV. During this period of data taking, each of the four LEP experiments recorded about 30 W pairs. The W mass determined by this measurement, combining the results of the four experiments, is $80.40^{+0.22}_{-0.20}$ GeV (see Figure 3).

At higher energies, the W mass is determined through kinematic reconstruction of the decay products. This is the method used for data taken at $\sqrt{s} = 172$ GeV, as well as for data taken at $\sqrt{s} = 183$ GeV. Each experiment recorded approximately 100 W pairs at 172 GeV and close to 800 W pairs at 183 GeV. The W mass determined from the data collected at 172 GeV is 80.53 ± 0.18 GeV; combining it with the result from the measurement at 161 GeV yields a LEP average of the W mass of

$$\boxed{m_W = 80.48 \pm 0.14 \text{ GeV}.}$$

No result from the data taking at 183 GeV was available at the time of writing.

In addition, the LEP experiments determine the W-pair cross section also at energies above the threshold. These measurements are in excellent agreement with the Standard Model and show strong support for the existence of all of the three production channels mentioned above (see Figure 4).

5 Radiative Corrections and Constraints on the Standard Model

The high precision with which the LEP experiments measure the directly observable parameters of the Standard Model makes them sensitive also to parameters that appear virtually in some of the radiative corrections at LEP energies. If one assumes the validity of the Standard Model, the radiative effects can be measured and used to put constraints on these parameters. The sensitivity of the LEP experiments to radiative effects is illustrated in Figure 5. It was demonstrated by the highly successful prediction of the mass of the top quark before the top quark was discovered and its mass measured directly at the Tevatron: The last prediction from precision measurements before the top quark was observed at the Tevatron in 1994 was $m_t = 174 \pm 11^{+17}_{-19}$ GeV [11]; averaged results from the CDF and DØ collaborations give a current top mass of 175.6 ± 5.5 GeV [12], [13], [14].

5.1 Important Radiative Effects

The radiative effects that are important to the LEP experiments can be classified in different categories (see, e.g., [15], [16], [17], [18]):

- One large group of corrections are those that arise from pure QED effects, i.e., emission of real or virtual photons. They depend on energies, experimental cuts, etc., but can be calculated within the framework of QED. As mentioned in Section 2.1, the method to take these corrections into account is to convolute Eq. 1 by a radiator function before the lineshape parameters are extracted.

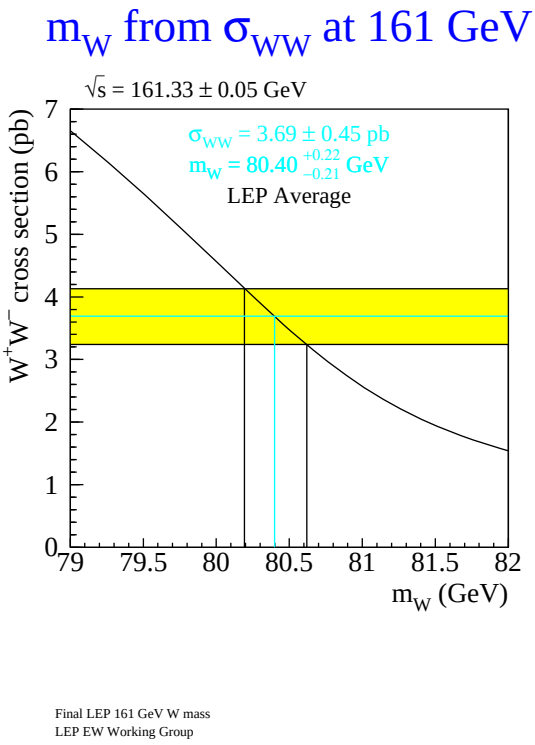

Figure 3: The determination of the mass of the W boson, m_W, from the cross section for W-pair production, σ_{WW}, at a centre-of-mass energy of 161 GeV. The curve shows the Standard-Model prediction for the cross section as a function of the W mass. The shaded band shows the measured cross section with its uncertainty.

- A second group pertains to the running of the QED coupling constant, α, due to the photon self energy:

$$\alpha \to \alpha(m_Z^2) = \frac{\alpha(0)}{1 - \Delta\alpha(m_Z^2)}. \tag{17}$$

The value of α at the Z^0 pole is an important input parameter to the precision electroweak measurements. Unfortunately, however, it is not known with great precision. The contribution from leptons to the photon self energy can be calculated analytically and is well known. The contribution from quarks is not entirely calculable due to uncertainty of the light quark masses; instead it is measured experimentally through integration of

$$R_h \equiv \frac{\sigma\left(e^+e^- \to \text{hadrons}\right)}{\sigma\left(e^+e^- \to \mu^+\mu^-\right)} \tag{18}$$

over $\sqrt{s}$. The largest uncertainty comes in the contribution from the low-energy range: More than 75% of the error comes from the range $1 \leq \sqrt{s} \leq 5$ GeV [19].

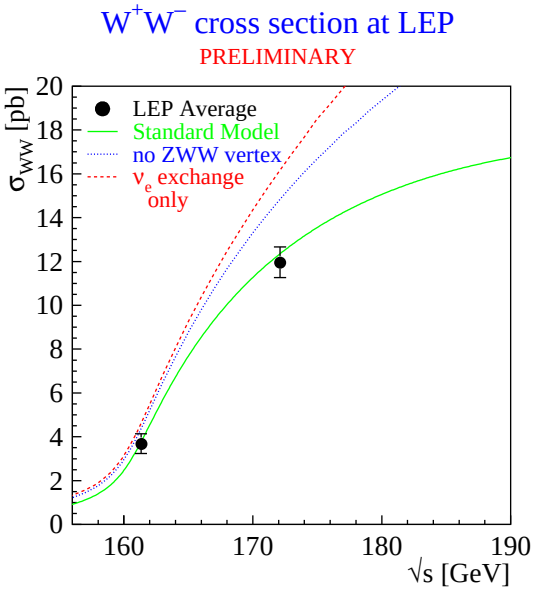

Figure 4: The cross section for W-pair production, σ_{WW}, as a function of the centre-of-mass energy. The dots show the LEP averages at 161 and 172 GeV. The solid curve shows the Standard-Model prediction when all three production channels are included (s-channel exchange of a γ or a Z^0 and t-channel exchange of a neutrino ν_e); the dotted curve shows the prediction if the ZWW coupling did not exist, and the dashed curve shows the prediction if only t-channel neutrino exchange existed.

- Loop corrections to Z^0 and W propagators give rise to corrections to the ρ parameter,

$$\rho = \frac{m_W^2}{\cos^2\theta_W m_Z^2}, \tag{19}$$

  which is equal to 1 at tree level. This group contains corrections that are sensitive to the top mass with a quadratic dependence:

$$\Delta\rho_t \sim \frac{m_t^2}{m_Z^2}.$$

  There is also sensitivity to the Higgs mass, although this dependence is much weaker; it is only logarithmic:

$$\Delta\rho_H \sim \log\frac{m_H^2}{m_Z^2}.$$

  However, the LEP experiments have now reached a level of sensitivity high enough for the constraints on the Higgs mass to be interesting, despite the weak dependence.

- Corrections to the $Z \to b\bar{b}$ vertex are sensitive to the top mass, with a quadratic dependence:

$$\delta_{vb} \sim \frac{m_t^2}{m_Z^2},$$

  where δ_{vb} is given by $\Gamma_{bb} = \Gamma_{dd}\,(1 + \delta_{vb})$.

5.2 Measurements

The Standard-Model parameters that are determined through radiative corrections at LEP are the mass of the top quark, the strong coupling constant $\alpha_s(m_Z^2)$ and either the mass of the Higgs boson or that

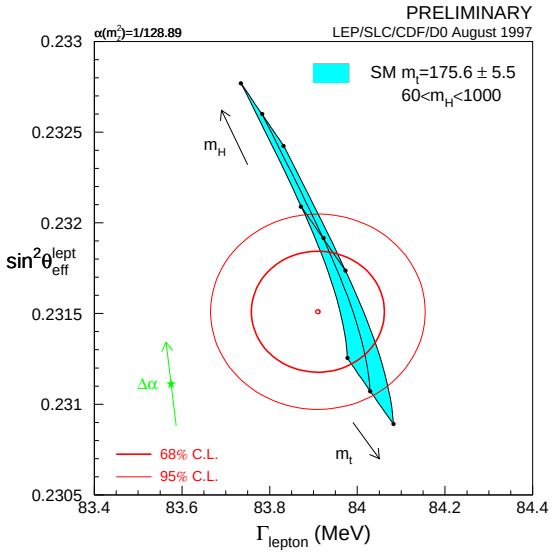

Figure 5: Contours of 68% and 95% probability of the effective electroweak mixing angle (LEP+SLD) *vs.* the leptonic partial width. The shaded area shows the Standard-Model prediction for a top mass of $m_t = 175 \pm 5.5$ GeV and a Higgs mass $m_H = 300^{+700}_{-240}$ GeV; the arrows indicate the directions of increasing top and Higgs masses. The star shows the Standard-Model prediction if all the electroweak radiative corrections except the running of α are left out. The arrow on the star indicates the influence of an uncertainty of one standard deviation on $\alpha(M_Z^2)$.

of the W boson. Different fit strategies are used to determine the different parameters. Three examples showing how m_H, m_t and m_W are determined are given here:

- An indirect measurement of m_t and m_W is compared to direct measurements at LEP2 and the Tevatron. The indirect measurement uses data from LEP, SLD and neutrino-scattering experiments, excluding data on m_W; m_W and m_t are left as free parameters in the fit. The indirect and the direct measurements are compatible, which implies stringent limits on physics beyond the Standard Model (see Figure 6).
- The Higgs mass is constrained in a fit that uses all LEP data, including m_W from LEP2; only m_t and m_H are left free in the fit.
- The best constraint on the Higgs mass is obtained from a fit using all available electroweak data from not only LEP but also SLD, $p\bar{p}$ colliders and neutrino-scattering experiments, notably the top mass from the Tevatron.

The results of the two different fits of the Higgs mass are shown in Figure 7. The fit to LEP data only shows a preference for a light Higgs boson and a light top quark. The fit to all data yields a Higgs mass of

$$\boxed{m_H = 115^{+116}_{-66}\ \text{GeV}.}$$

Figure 8 shows $\Delta\chi^2 = \chi^2 - \chi^2_{min}$ as a function of the Higgs mass for the fit using all available data. With the error on the theoretical calculations taken into account, this fit yields a one-sided confidence level for the Higgs mass of

$$\boxed{m_H < 420\ \text{GeV at } 95\%\ \text{C.L.}}$$

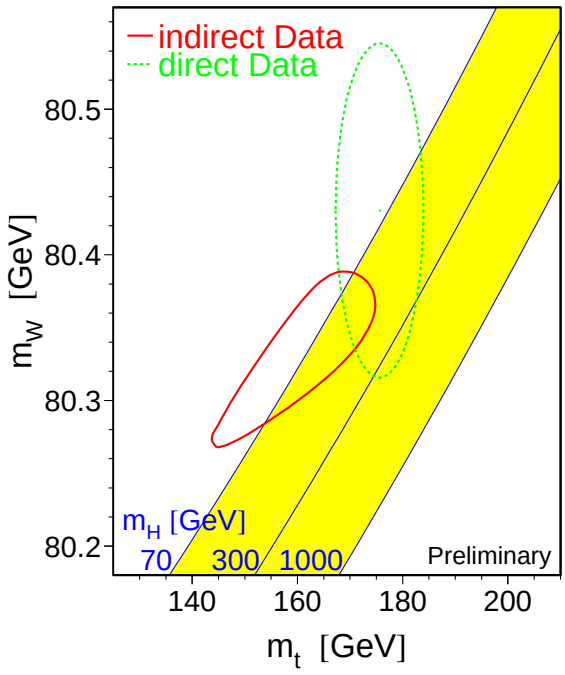

Figure 6: Contours of 68% probability for the W mass, m_W, *vs.* the top mass, m_t. The solid curve shows the result of the indirect measurement where data from LEP, SLD and neutrino-scattering experiments have been used. The dashed curve shows the results of direct measurements of m_W and m_t at LEP2 and at the Tevatron. The shaded region shows the Standard-Model relationship for the masses as a function of the Higgs mass. The LEP data indicate a preference for a light top quark and a light Higgs boson.

6 Conclusions and Outlook

The successful operation of LEP over several years has allowed precise tests of the Standard Model to be performed. The $SU(2)_L \times U(1)$ structure has been extremely well verified, with no deviation at the 10^{-3} level [9]. The radiative corrections have also been very well confirmed. The prediction of the top mass before it was discovered at the Tevatron in 1994 was indeed very successful. The predictions of the Higgs mass, together with the limits set by direct searches, are now becoming highly interesting and indicate the importance of the remaining years of data taking at high energies with LEP.

The LEP1 era ended in 1995. Some analyses are still unfinished, notably those of the τ polarisation and the quark forward-backward asymmetries. The results of what was probably the final LEP1 energy calibration were presented recently, and these results are now being taken into account by the experiments. At LEP2, improvements of the measurement of the W mass down to uncertainties of $\Delta m_W = 25 - 50$ MeV should be possible [1], [9]. When the LEP2 results are combined with those of the Tevatron, an uncertainty of $\Delta m_W \simeq 20$ MeV should be within reach [16].

The Higgs mass remains the only free parameter of the Standard Model still to be measured. Improvements in the prediction of the Higgs mass by precision electroweak tests will require improvements in all of the following [9], [16]:

- The determination of the top mass. This should come with increased statistics when the Tevatron restarts in 1999 after its upgrade.

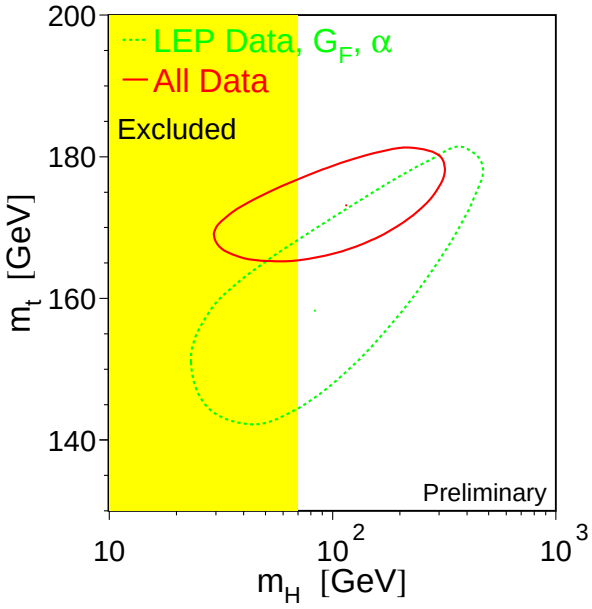

Figure 7: Contours of 68% probability for the top mass, m_t, *vs.* the Higgs mass, m_H. The dashed curve shows the result of the fit to LEP data only, with m_t and m_H left as free parameters. The solid curve shows the result of the fit using data from LEP, SLD, $p\bar{p}$ colliders and neutrino-scattering experiments, including the data on the top mass from the Tevatron. The shaded area shows the mass region excluded by direct searches. The LEP data again show a slight preference for a light top quark and a light Higgs boson.

- The measurements of $\sin^2\theta_W^{eff}$. The improvements will come from some unfinished analyses at LEP1 and from better statistics at SLD; the uncertainty can be expected to be reduced by a factor of 1.5 at most.
- The determination of $\alpha(m_Z^2)$. This is the most uncertain ingredient in an improved constraint on the Higgs mass. The improved value of $\alpha(m_Z^2)$ would come through measurements of low-energy hadronic cross sections, possibly from BES or Novosibirsk.

7 Acknowledgements

The author is greatly indebted to A. Blondel and A. Olchevski for their invaluable suggestions and help in selecting material. The underlying work of the LEP Electroweak Working Group in averaging the results of the four LEP experiments provided the platform for this presentation; most of the numbers and all of the graphs presented here were produced by them.

References

[1] D. Schaile in N. Ellis, M. Neubert, eds., CERN Yellow Report 97-03, p. 199.
[2] D. Ward, Talk given at the International Europhysics Conference on High Energy Physics, Jerusalem 1997.
[3] G. Quast, Talk given at the International Europhysics Conference on High Energy Physics, Jerusalem 1997.
[4] LEP Electroweak Working Group, Preprint CERN-PPE/96-183.
[5] LEP Polarization Collaboration, Preprint CERN-PPE/92-49.

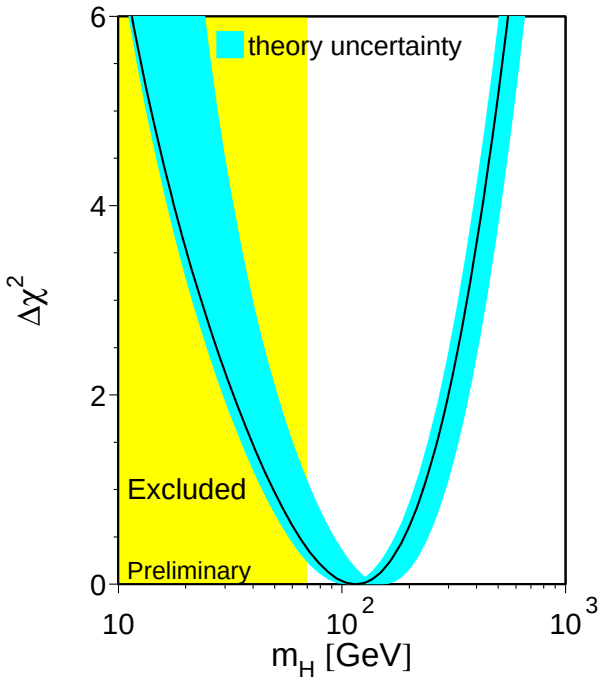

Figure 8: $\Delta\chi^2 = \chi^2 - \chi^2_{min}$ as a function of the Higgs mass, m_H. The curve shows the result of the fit using all available electroweak data, including the top mass from the Tevatron. The dark shaded region represents an estimate of the theoretical uncertainty due to missing higher-order corrections. The light shaded area shows the mass region excluded by direct searches.

[6] P. Langacker, ed., *Advanced Series on Directions in High Energy Physics,* vol. 14: *Precision Tests of the Standard Electroweak Model*, World Scientific Publishing Co., Singapore 1995.

[7] A. Blondel in [6], p. 277.

[8] A. Blondel in T. Riemann, J. Blümlein, eds., *Proceedings of the Zeuthen Workshop on Elementary-Particle Theory: Physics at LEP200 and Beyond*, Nucl. Phys. B, Proc. Suppl. 37B (1994) 3.

[9] A. Blondel in T. Ferbel, ed., *Techniques and Concepts of High Energy Physics IX*, p. 381, Plenum Press, New York 1997.

[10] A. Blondel *et al.* in *Proceedings of the 1997 Particle Accelerator Conference PAC '97,* Vancouver 1997.

[11] B. Pietrzyk, Talk given at the XXIX Rencontres de Moriond, Méribel 1994.

[12] CDF Collaboration, J. Lys, Talk given at the 28th International Conference on High Energy Physics ICHEP '96, Warsaw 1996; to appear in the proceedings.

[13] DØ Collaboration, S. Protopopescu, Talk given at the 28th International Conference on High Energy Physics ICHEP '96, Warsaw 1996; to appear in the proceedings.

[14] The results from CDF and DØ have been averaged together assuming a 3 GeV common systematic error.

[15] D. Schaile in [6], p. 215.

[16] A. Blondel, To appear in *Perspectives in Higgs Physics II,* ed. G.L. Kane, World Scientific Publishing Co.

[17] R.M. Barnett *et al.*, Physical Review D54, 1(1996).

[18] W. Hollik in [6], p. 37; p. 117.

[19] P. Renton in C.P. Zheng, H.S. Chen, eds., *Proceedings of the 17th International Symposium on Lepton-Photon Interactions LP '95*, p. 35, World Scientific Publishing Co., Singapore 1996.

[20] A. Blondel in CERN Yellow Report 92-06, p. 23.
[21] R. Miquel in CERN Yellow Report 92-06, p. 267.
[22] A. Olchevski in J. Lemmone, C. Vander Velde, F. Verbeure, eds., *Proceedings of the International Europhysics Conference on High-Energy Physics EPS-HEP '95*, World Scientific Publishing Co., Singapore 1996.
[23] A. Blondel, Private communication.
[24] A. Olchevski, Private communication.
[25] D. Treille in [6], p. 325.
[26] P. Langacker in [6], p. 15; p. 883.